Production of K^+K^- pairs in proton-proton collisions at 2.83 GeV

Q. J. Ye,[1,2,*] M. Hartmann,[2,†] Y. Maeda,[3] S. Barsov,[4] M. Büscher,[2] D. Chiladze,[2,5] S. Dymov,[6,7] A. Dzyuba,[4] H. Gao,[1] R. Gebel,[2] V. Hejny,[2] A. Kacharava,[2] I. Keshelashvili,[8] Yu. T. Kiselev,[9] A. Khoukaz,[10] V. P. Koptev,[4,‡] P. Kulessa,[11] A. Kulikov,[7] B. Lorentz,[2] T. Mersmann,[10] S. Merzliakov,[2,7] S. Mikirtytchiants,[2,4] M. Nekipelov,[2] H. Ohm,[2] E. Ya. Paryev,[12] A. Polyanskiy,[2,9] V. Serdyuk,[2,7] H. J. Stein,[2] H. Ströher,[2] S. Trusov,[13,14] Yu. Valdau,[2,15] C. Wilkin,[16] and P. Wüstner[17]

[1]*Department of Physics and Triangle Universities Nuclear Laboratory, Duke University, Durham, North Carolina 27708, USA*
[2]*Institut für Kernphysik and Jülich Centre for Hadron Physics, Forschungszentrum Jülich, D-52425 Jülich, Germany*
[3]*Research Center for Nuclear Physics, Osaka University, Ibaraki, Osaka 567-0047, Japan*
[4]*High Energy Physics Department, Petersburg Nuclear Physics Institute, RU-188350 Gatchina, Russia*
[5]*High Energy Physics Institute, Tbilisi State University, GE-0186 Tbilisi, Georgia*
[6]*Physikalisches Institut, Universität Erlangen-Nürnberg, D-91058 Erlangen, Germany*
[7]*Laboratory of Nuclear Problems, Joint Institute for Nuclear Research, RU-141980 Dubna, Russia*
[8]*Department of Physics, University of Basel, CH-4056 Basel, Switzerland*
[9]*Institute for Theoretical and Experimental Physics, RU-117218 Moscow, Russia*
[10]*Institut für Kernphysik, Universität Münster, D-48149 Münster, Germany*
[11]*H. Niewodniczanski Institute of Nuclear Physics PAN, PL-31342 Cracow, Poland*
[12]*Institute for Nuclear Research, Russian Academy of Sciences, RU-117312 Moscow, Russia*
[13]*Institut für Kern- und Hadronenphysik, Helmholtz-Zentrum Dresden-Rossendorf, D-01314 Dresden, Germany*
[14]*Skobeltsyn Institute of Nuclear Physics, Lomonosov Moscow State University, RU-119991 Moscow, Russia*
[15]*Helmholtz-Institut für Strahlen- und Kernphysik, Universität Bonn, D-53115 Bonn, Germany*
[16]*Physics and Astronomy Department, UCL, London WC1E 6BT, United Kingdom*
[17]*Zentralinstitut für Elektronik, Forschungszentrum Jülich, D-52425 Jülich, Germany*

(Received 24 February 2012; published 30 March 2012)

Differential and total cross sections for the $pp \to ppK^+K^-$ reaction have been measured at a proton beam energy of 2.83 GeV using the COSY-ANKE magnetic spectrometer. Detailed model descriptions fitted to a variety of one-dimensional distributions permit the separation of the $pp \to pp\phi$ cross section from that of non-ϕ production. The differential spectra show that higher partial waves represent the majority of the $pp \to pp\phi$ total cross section at an excess energy of 76 MeV, whose energy dependence would then seem to require some s-wave ϕp enhancement near threshold. The non-ϕ data can be described in terms of the combined effects of two-body final state interactions using the same effective scattering parameters determined from lower energy data.

DOI: 10.1103/PhysRevC.85.035211 PACS number(s): 13.75.Jz, 14.40.Be, 25.40.Ep

I. INTRODUCTION

The phenomenological description of strangeness production in nucleon-nucleon collisions near threshold is complicated for a variety of reasons and these add to its general interest. The large mass changes involved are necessarily associated with short-range phenomena and therefore stress the importance of heavy meson exchange. Whether such exchanges are mainly of a strange or nonstrange nature is still an open question.

It is known that the scattering lengths in the Λp and K^-p systems are both very large and these will distort any spectra. Furthermore, important transitions, such as $\Sigma p \leftrightarrow \Lambda p$, mean that several of the final channels are strongly coupled. It is also possible that, because of such a coupling, the production of a heavy hyperon in $pp \to K^+p\Lambda(1405)$ might influence kaon pair production in the $pp \to ppK^+K^-$ reaction [1]. The only hope of being able to disentangle such effects is through having detailed experimental spectra in different kinematic variables.

In addition to explicit strangeness production one has to consider also hidden strangeness, such as that residing in the ϕ meson which, in the quark model, is mainly composed of $s\bar{s}$ pairs. The $pp \to pp\phi$ cross section might therefore be influenced by other strangeness production channels that are important at this energy. We know from the Okubo-Zweig-Iizuka (OZI) rule [2] that the ϕ production rate should be much lower than that of the ω meson in the $pp \to pp\omega$ channel. Some of the widely observed violations of this rule, such as, for example, in the ϕ/ω ratio measured in $p\bar{p}$ annihilation [3], might be understood if there were significant strangeness components in the nucleon. There are, however, alternative explanations in terms of modified meson exchange models [4,5]. The production of the ϕ meson in proton-nucleus collisions will clearly depend on the more elementary $pp \to pp\phi$ cross section and so this will also be an important ingredient in the understanding of proton-induced nuclear transparency measurements [6].

The production of the ϕ meson in pp collisions was studied in several theoretical papers within a simple one-meson-exchange model [7], including both mesonic and nucleonic current components [8–11], and also contributions from nucleon resonances [12–14]. However, the somewhat limited published data set is not sufficient to provide strong constraints

*qy4@phy.duke.edu
†m.hartmann@fz-juelich.de
‡Deceased

on the different models. It is the aim of the present paper to present detailed measurements of the $pp \to ppK^+K^-$ reaction at a beam energy of 2.83 GeV, where the cross sections for the production of the ϕ meson is cleanly separated from the non-ϕ.

We have previously published data on the $pp \to ppK^+K^-$ reaction [15,16] at excess energies with respect to the ϕ threshold, $\varepsilon_\phi = \sqrt{s} - (2m_p + m_\phi)c^2$, of 18.5, 34.5, and 76 MeV, where $\sqrt{s}$ is the total center-of-mass (c.m.) energy. The data on ϕ production at the lowest energy are consistent with the particles in the final state being all in relative S waves, with the only feature evident in the measured spectra coming from the strong proton-proton final state interaction (FSI). The lower statistics at the two higher energies were sufficient to extract total cross sections but it was hard to draw firm conclusions regarding the differential spectra which, on general grounds, are expected to be much richer than at $\varepsilon_\phi = 18.5$ MeV.

In the pioneering work of the DISTO collaboration, strong evidence was presented for the importance of higher partial waves in the $pp \to pp\phi$ reaction at $\varepsilon_\phi = 83$ MeV [17], but no attempt was made to make a consistent partial wave decomposition. The reason was in part because of the necessity to study in detail the structure of the non-ϕ K^+K^- background. We have since then shown [16] that, because of the K^-p final state interaction, the differential spectra for the non-ϕ contribution to the $pp \to ppK^+K^-$ reaction are strongly distorted. As a consequence, one needs full descriptions of both ϕ and non-ϕ components to extract credible partial wave parameters. When these are implemented in our current data set it is found that only a small amount of the total $pp \to pp\phi$ cross section at $\varepsilon_\phi = 76$ MeV corresponds to pure S-wave final states and this explains the nonobservation of the S-wave pp FSI enhancement in the results. However, the energy dependence of the total ϕ production cross section then seems to require some enhancement in the ϕp system at low invariant masses.

The distortion of the K^-p and K^-pp invariant mass spectra observed in the $pp \to ppK^+K^-$ reaction were very well parametrized by assuming factorized pair-wise final state interactions in the pp, K^-p, and K^+K^- systems with constant effective scattering lengths [16]. Furthermore, their inclusion led to a good description of the energy dependence of the total cross section, including the low energy COSY-11 data [18–20]. The distortions were in fact first identified in data taken below the ϕ threshold where selection of the non-ϕ contribution is automatic [20]. These distortions were well described by the FSI parameters used at higher energies but, taken in isolation, the error bars on the parameters extracted from these low energy data were very large [21].

We here present much more precise differential data for the $pp \to ppK^+K^-$ reaction at a beam energy of $T_p = 2.83$ GeV ($\varepsilon_\phi = 76$ MeV) obtained using the COSY-ANKE spectrometer. These will challenge the theoretical models that can describe well the energy dependence of the $pp \to pp\phi$ total cross sections. Currently few of the experimental spectra are calculated in any of the phenomenological approaches.

The paper is organized as follows. We first describe the experimental setup and data analysis in Sec. II. The detailed phenomenological parametrizations developed for ϕ and non-ϕ K^+K^- production needed to make the acceptance corrections are described here. The resulting differential distributions for ϕ production are presented in Sec III, with the integrated cross sections for all the $pp \to ppK^+K^-$ data being given in Sec. IV. The distortions in the non-ϕ differential cross sections arising from the various final state interactions are discussed in Sec. V, followed by our conclusions in Sec. VI.

II. EXPERIMENT AND DATA ANALYSIS

The experiment was performed at the Cooler Synchrotron (COSY) of the Forschungszentrum Jülich [22] using the ANKE magnetic spectrometer [23,24] that is located at an internal target station of the storage ring. ANKE contains three dipole magnets; *D1* and *D3* divert the circulating beam onto the target and back into the COSY ring, respectively, while *D2* is the analyzing magnet. There are detection systems placed to the right and left of the beam that register positively and negatively charged ejectiles, respectively, while fast positive particles are measured in the forward detector. Both the positive and negative side detectors consist of sets of start and stop scintillation counters for time-of-flight (TOF) measurements and two multiwire proportional chambers (MWPCs) utilized for particle momentum reconstruction. Two layers of scintillation hodoscopes and three MWPCs are incorporated in the forward detector which, in addition to studying a fast proton from the $pp \to ppK^+K^-$ reaction, is also used to measure subsidiary reactions that are needed to determine the luminosity [15,23,25]. A high density hydrogen cluster-jet target [26] was employed in the experiment.

Particle identification relied on momentum determination and time-of-flight measurements [15,16,27]. The time differences were calibrated by using, respectively, $\pi^+\pi^-$ and π^+p pairs for the negative and forward STOP counters with respect to the positive STOP counters, described in detail in Ref. [24]. The kaon detection efficiency depends on the particle's momentum and varied between 92% and 98%, whereas that for the forward-going protons was about 96%. The uncertainties in the efficiency estimates were about 3%.

The $pp \to ppK^+K^-$ reaction was identified through a triple coincidence involving the detection of a K^+K^- pair and a forward-going proton, with the additional requirement that the missing mass of the K^+K^-p system be consistent with that of the proton. In the off-line analysis, positive kaons were selected by a dedicated K^+ detection system using the TOF information between the START and the STOP counters [27]. The K^- and forward-going protons were then selected simultaneously using the time-of-flight differences, as described in detail in Ref. [24].

All time-of-flight selections, as well as the identification of the K^+, were performed within $\pm 3\sigma$ ranges. A similar cut was also made in the missing-mass distribution of the detected K^+K^-p shown in Fig. 1. The fraction of misidentified events inside the $\pm 3\sigma$ ($\sigma = 4.7$ MeV/c^2) cut window around the proton mass was estimated to be about 11.5%, which was subtracted in the analysis using weighted data from the side bands, as parametrized by the solid line. Any ambiguity in this

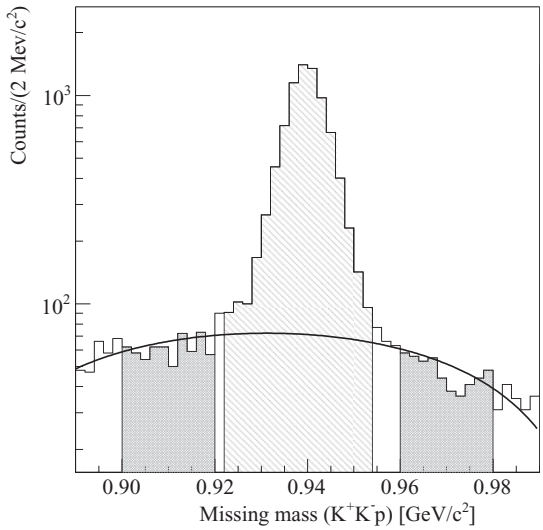

FIG. 1. The K^+K^-p missing-mass distribution in the $pp \to pK^+K^-X$ reaction at $T_p = 2.83$ GeV. The hatched histogram shows the cuts used for the selection of the nondetected proton. The solid line, which is a second-order polynomial curve, was used in the analysis to estimate the background contribution under the proton peak.

procedure is less than 3% and is considered as one source of systematic uncertainties in the analysis.

Having identified good $pp \to ppK^+K^-$ events, these were binned in terms of the K^+K^- invariant mass, $\mathrm{IM}_{K^+K^-}$, and the corresponding results are shown in Fig. 2. A clear ϕ

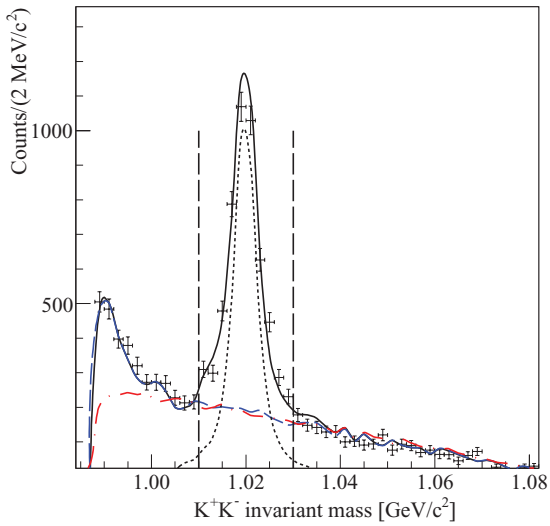

FIG. 2. (Color online) The raw K^+K^- invariant mass distribution, $\mathrm{IM}_{K^+K^-}$ (points), is compared with the distribution of events obtained in a Monte Carlo simulation (curve). The error bars indicate only the statistical uncertainties. The dashed blue curve shows the non-ϕ contributions within the fitted parametrization, the dashed-dotted red curve the four-body phase-space simulation of ppK^+K^-, and the dotted curve the ϕ contributions. The solid line is the incoherent sum of the ϕ and non-ϕ contributions. The vertical lines indicate the cuts used for the separation of the ϕ-rich and non-ϕ regions. The fluctuations reflect the Monte Carlo sampling effects.

peak is observed above a slowly varying background. The experimental data were then divided into two samples, a ϕ-rich region where $1.01\ \mathrm{GeV}/c^2 < \mathrm{IM}_{K^+K^-} < 1.03\ \mathrm{GeV}/c^2$ and a non-ϕ (the rest) region. The model-independent acceptance estimate method used in our earlier work [15,16], cannot be applied in the present analysis because, at this higher excess energy, the number of zero elements in the acceptance matrix is significant and this leads to large fluctuations. Phenomenological parametrizations that describe well the experimental data in both the ϕ and non-ϕ regions must therefore be relied upon to perform the necessary acceptance corrections.

We start the analysis with the kaon pair production away from the ϕ region because it is crucial to master this contribution to understand the background under the ϕ peak. The ansatz in our previous work on non-ϕ production [16] was taken as the basis of the simulation. Here it was assumed that the overall enhancement factor was the product of enhancements in the pp and two K^-p systems:

$$F = F_{pp}(q_{pp}) \times F_{Kp}(q_{Kp_1}) \times F_{Kp}(q_{Kp_2}), \qquad (1)$$

where q_{pp}, q_{Kp_1}, and q_{Kp_2} are the magnitudes of the relative momenta in the pp and the two K^-p systems, respectively. Note that it is believed that the K^+p interaction might be weakly repulsive and, if so, its effects would be interpreted as extra attraction in the K^-p system.

Using an effective K^-p scattering length of $a_{K^-p} = (0 + 1.5i)$ fm [16], together with an additional weight of $1 + 2.0\cos^2\theta$ on the polar angle of the K^+K^- system in the overall c.m. system, the invariant mass distributions can be described very well, except for the very low K^+K^- invariant masses, $\mathrm{IM}_{K^+K^-} < 995\ \mathrm{MeV}/c^2$. In this region there are small residual effects associated with $K\bar{K}$ final state interactions [28], to which we shall return later.

Seven degrees of freedom are required to parametrize the unpolarized ppK^+K^- final state and these were chosen to be four angles, the K^+K^- and K^+K^-p invariant masses, and the relative momentum of the protons in the pp system. Distributions in these seven variables were generated inside the ANKE acceptance and compared with the experimental data for non-ϕ data in Fig. 3. It is evident that the description of the nonresonant $pp \to ppK^+K^-$ reaction at $T_p = 2.83$ GeV is very satisfactory and the same is true for the K^+K^- invariant mass distribution of Fig. 2 when the ϕ contribution is added incoherently.

Turning now to ϕ production in proton-proton collisions, the only amplitude that survives at threshold corresponds to the $^3P_1 \to {}^1S_0 s$ transition. We here denote the final state by $^{2S+1}L_J\ell$, where S, L, and J represent the total spin, orbital angular momentum, and total angular momentum of the pp system, respectively, and ℓ the orbital angular momentum of the ϕ relative to the pp system. Our previous analysis indicates that the differential cross section at an excess energy $\varepsilon_\phi = 18.5$ MeV is dominantly $L = 0$, with a clear effect coming from the pp final state interaction [15].

In contrast, significant contributions from higher partial waves were suggested by the DISTO data at $\varepsilon_\phi = 83$ MeV [17], where the differential cross sections as functions of the proton momentum in the pp reference frame and the momentum of

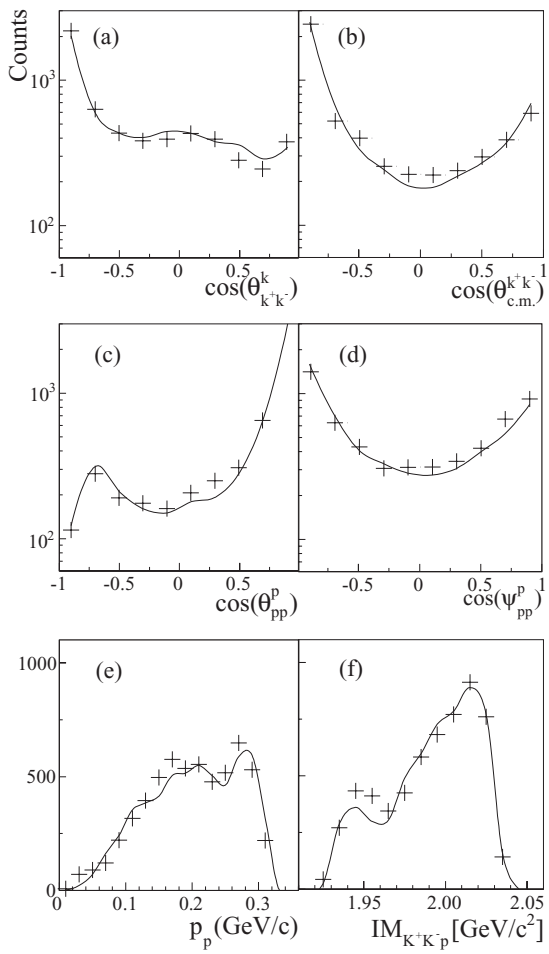

FIG. 3. Differential distributions of experimental (points) and simulated (curves) yields for kaon pair production in the $pp \to ppK^+K^-$ reaction at $T_p = 2.83$ GeV for the non-ϕ regions ($IM_{K^+K^-} < 1.01$ GeV/c^2 or $IM_{K^+K^-} > 1.03$ GeV/c^2). Vertical bars represent the statistical uncertainties and horizontal ones the bin widths. The individual panels are (a) the cosine of the polar angle of the K^+ in the K^+K^- reference frame, (b) the polar angle of the kaon pairs in the overall c.m. frame, (c) the polar angle of the emitted proton in the pp reference frame relative to the beam direction, (d) the polar angle of the proton in the pp reference frame relative to the direction of the kaon pair, (e) the proton momentum in the pp reference frame, and (f) the K^+K^-p invariant mass distribution.

ϕ meson in the c.m. system were interpreted as reflecting the importance of Ps and Sp final waves, respectively. The anisotropy in the helicity distribution shows the necessity also for a Pp contribution.

There are several possible transitions that could lead to a $pp\phi$ final state and we keep only typical ones in our model description, where the spin-averaged squared transition matrix element is written as

$$\overline{|M|^2} = A_{Ss}\,(\hat{k}\times\hat{K})^2 + A_{Ps}\,\vec{p}^{\,2} + A_{Pp}(\vec{q}\cdot\vec{p}\,)^2 + A_{Sp}[3(\vec{q}\cdot\hat{K})^2 - \vec{q}^{\,2}]. \quad (2)$$

The momentum of the beam proton and the ϕ meson in the overall c.m. system are denoted by $\vec{K}$ and $\vec{q}$, respectively, $\vec{k}$ represents the momentum of decay kaons in the ϕ reference frame, and $\vec{p}$ is the relative momentum in the final pp system.

TABLE I. Values of the model parameters of Eq. (2) deduced by comparing the simulations with data in the ϕ region. The momenta are measured in GeV/c. All the parameters are normalized to $A_{Ss} = 1$ and the corresponding uncertainty of ± 0.25 is not included.

Parameter	Fit value
A_{Ss}	1.0
A_{Sp}	9.9 ± 1.8
A_{Ps}	143 ± 4
A_{Pp}	293 ± 21

Apart from the explicit momentum factors, we assume that the coefficients $A_{L\ell}$ in Eq. (2) are constant except that, at low invariant masses, the final pp system in the $^1S_0$ state is subject to a very strong final state interaction. The A_{Ss} and A_{Sp} contributions in Eq. (2) were therefore multiplied by an enhancement factor which was calculated using the Jost function,

$$F_{pp}(q_{pp}) = |J(q_{pp})|^{-2} = \frac{q_{pp}^2 + \beta^2}{q_{pp}^2 + \alpha^2}\,, \quad (3)$$

where we take $\alpha = 0.1$ fm^{-1} and $\beta = 0.5$ fm^{-1} [16]. The Coulomb interaction was neglected and, crucially, no attempt was made to include a final state interaction in the ϕp system.

A Monte Carlo phase-space simulation was written, based on GEANT4 [29], which took into account the detector efficiency, resolution and kaon decay probability. Contributions from the phenomenological parametrizations for ϕ and non-ϕ production were then included as weights. The ϕ meson was taken to have a Breit-Wigner form with a width of $\Gamma = 4.26$ MeV/c^2 [30], convoluted with a resolution width of $\sigma \simeq 1$ MeV/c^2. The values of the coefficients $A_{L\ell}$ in Eq. (2) were determined by minimizing χ^2 in the difference between the simulated and experimental spectra, and the results are shown in Table I. The resulting descriptions of the experimental data in Figs. 2–4 are very good and certainly adequate for carrying out the acceptance corrections.

The fits of the parametrizations to the experimental data allow the extraction of the differential and total cross sections for both ϕ and non-ϕ kaon pair production. The luminosity needed for this analysis was determined on the basis of the pp elastic scattering data that were taken in parallel, using the forward detector [16]. The associated systematic uncertainty is estimated to be 7%. Systematic uncertainties also arise from the background subtraction, tracking efficiency, and the model-dependent acceptance corrections. The latter were estimated from the differences between the distributions corrected by the parametrization and those corrected by phase space. As the observed distributions deviate significantly from phase space, such estimates provide upper limits on these uncertainties.

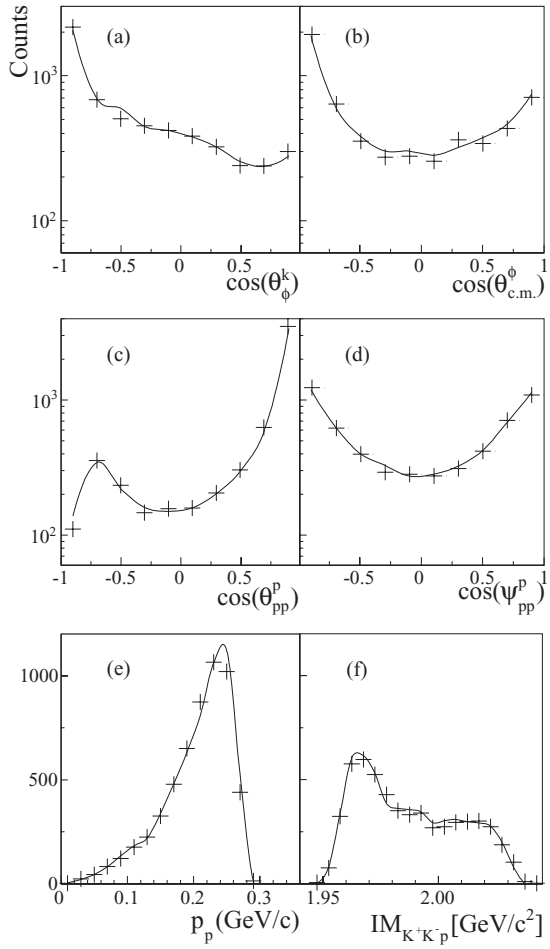

FIG. 4. The differential distributions of yields in the ϕ region ($1.01\,\mathrm{GeV}/c^2 < \mathrm{IM}_{K^+K^-} < 1.03\,\mathrm{GeV}/c^2$) for the $pp \to ppK^+K^-$ reaction at $T_p = 2.83$ GeV, where the points are experimental and the curves represent simulations. The notations for the six panels are the same as those in Fig. 3.

III. DIFFERENTIAL CROSS SECTIONS FOR ϕ PRODUCTION

The angular distributions for the $pp \to pp\phi$ reaction measured in this experiment and those of DISTO [17] are shown in Fig. 5. These distributions must be symmetric about $\cos\theta = 0$ and the data can be parametrized in the form,

$$\frac{d\sigma}{d\Omega} = a\,[1 + b\,P_2(\cos\theta)]\,. \tag{4}$$

The numerical values of the coefficients obtained from fitting the data are reported in Table II.

In the near-threshold region where the Ss final state dominates the ϕ meson spin must lie along the beam direction. The polar angular distribution of the decay kaons in the ϕ meson rest frame should then display a $\sin^2\theta_\phi^K$ distribution, where θ_ϕ^K is the angle of a daughter kaon from the ϕ decay in the ϕ rest frame. The data at $\varepsilon_\phi = 18.5$ MeV [15] are consistent with such a dependence and deviations from this behavior are a sign of higher partial waves.

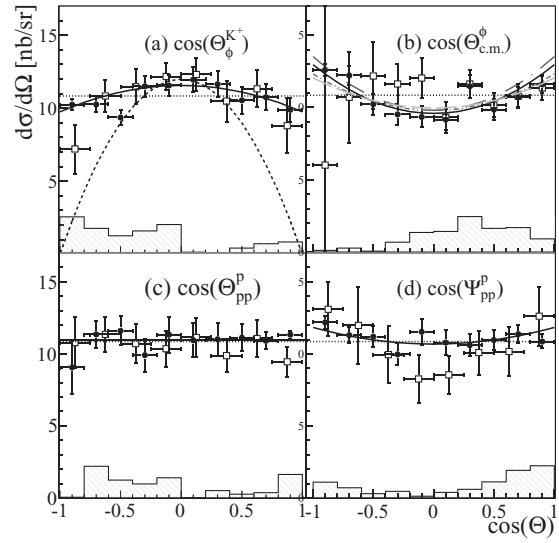

FIG. 5. (Color online) Angular distributions of the $pp \to pp\phi$ reaction obtained in this experiment (solid circles), where the systematic uncertainties are shown by the hatched histograms, compared with the scaled DISTO data (open squares) [17]. The dotted curves represent isotropic distributions whereas the solid ones show fits to the ANKE results. (a) The distribution with respect to the cosine of the K^+ polar angle in the ϕ rest frame (decay angle). The dashed curve demonstrates a $\sin^2\theta_\phi^K$ behavior. (b) The distribution in the ϕ polar angle in the overall c.m. system. The blue (dot-dashed), red (dot-dot-dashed), and green (dashed) curves are typical theoretical predictions from Refs. [9,11,13], respectively. (c) The distribution in the proton polar angle in the pp reference frame relative to the incident proton direction (Jackson angle). (d) The distribution of the proton polar angle in the pp reference frame relative to the ϕ direction (helicity angle).

Quite generally, the differential cross section is of the form,

$$\frac{d\sigma}{d\Omega} \propto \left[(1-\rho_{00})\sin^2\theta_\phi^K + 2\rho_{00}\cos^2\theta_\phi^K\right], \tag{5}$$

where $\rho_{00} = (1 + b_K)/3$ is a spin density matrix element. From the value of b_K given in Table II it is seen that the ANKE results correspond to $\rho_{00} = 0.30 \pm 0.01$, which is close to the unpolarized value of $\frac{1}{3}$. This is to be compared with the value of $\rho_{00} = 0.23 \pm 0.04$ reported by DISTO at the marginally higher $\varepsilon_\phi = 83$ MeV [17] where, in both cases, only statistical errors are quoted. These are model-independent proofs that higher partial waves are important at even relatively modest excess energies. A similar conclusion is reached in a study of the available $pn \to d\phi$ data [31].

The angular distribution of the ϕ meson in the overall c.m. frame shown in Fig. 5(b) is symmetric within experimental uncertainties. The ANKE data show a stronger anisotropy than those of DISTO, as indicated by the larger b parameter in Table II, but the error bars of the DISTO data are significant. Theoretical calculations [9,11,13] can describe a nonisotropy in the experimental data reasonably well, as shown in Fig. 5(b). The angular distribution is expected to be isotropic when the mesonic current is dominant, whereas the nucleonic current leads to a $\cos^2\theta$ distribution. The angular distribution might

TABLE II. Values of the coefficients of Eq. (4) for the K^+ decay angle with respect to the beam direction, the c.m. production angle, and the helicity angle, deduced by fitting the data of ANKE and DISTO [17]. The DISTO data have been scaled by 0.7 to allow a direct comparison of the two sets of results.

	ANKE		DISTO (scaled by 0.7)	
	a [nb/sr]	b	a [nb/sr]	b
$\cos\theta^K_\phi$	10.96 ± 0.23	-0.11 ± 0.04	10.78 ± 0.50	-0.27 ± 0.08
$\cos\theta^\phi_{\text{c.m.}}$	10.71 ± 0.21	0.21 ± 0.04	10.81 ± 0.45	0.07 ± 0.07
$\cos\Psi^p_{pp}$	11.06 ± 0.22	0.07 ± 0.04	10.64 ± 0.64	0.30 ± 0.14

therefore provide some information on the $NN\phi$ coupling constant [10,11].

It could be interesting to compare our or the DISTO results of Table II with the analogous measurement at COSY-TOF of the $pp \to pp\omega$ reaction at an excess energy of 92 MeV [32]. Unfortunately, the error bars in the ω angular distribution, $1.0 + (0.23 \pm 0.26)P_2(\cos\theta)$, are too large to draw any useful conclusions as to whether the shapes are similar or not.

The distribution in the proton polar angle measured in the pp reference frame relative to the beam direction is nearly isotropic, as shown in Fig. 5(c). This is consistent with the DISTO results. On the other hand, the analogous observable relative to the ϕ direction shown in Fig. 5(d) has some anisotropy. This feature, which was also seen in the DISTO data [17], is evidence for a contribution from a Pp final wave.

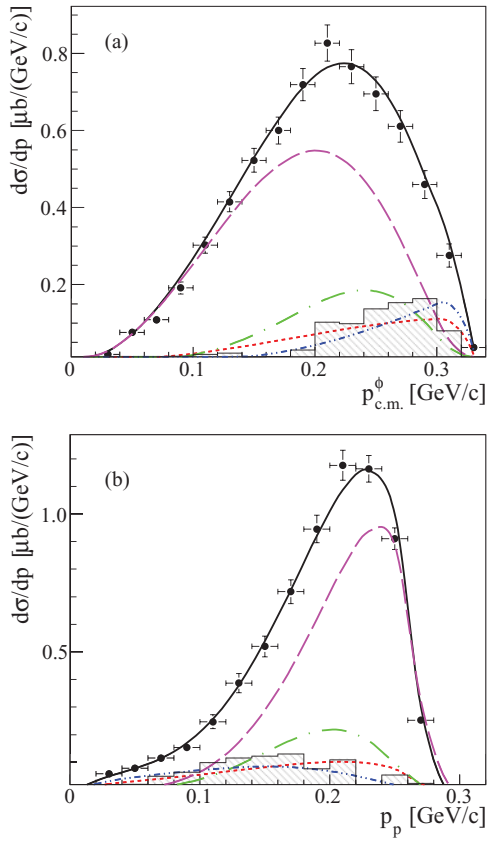

FIG. 6. (Color online) (a) Differential cross section for the $pp \to pp\phi$ reaction as a function of the momentum of the ϕ meson in the c.m. system. (b) Differential cross section for the $pp \to pp\phi$ reaction as a function of the proton momentum in the pp rest frame. The systematic uncertainties are shown by the hatched histograms. The fitted contributions from the Ss (dotted red curve), Sp (double dotted-dashed blue curve), Ps (dashed magenta curve), Pp (dashed-dotted green curve) are presented within the parametrization of Eq. (2).

In neither the ANKE data at $\varepsilon_\phi = 76$ MeV nor those of DISTO at $\varepsilon_\phi = 83$ MeV is there any sign of the FSI enhancement in the proton-proton relative momentum spectrum. The lack of such an effect can be understood by looking at the momentum distributions of the ϕ meson in the c.m. system and relative momentum distribution of the final protons in the pp reference frame that are shown in Fig. 6. The contributions of the different partial waves obtained by fitting Eq. (2) to the ANKE data are also indicated. From these it is seen that, within the given parametrization, the pp P waves are completely dominant and this reduces considerably the influence of the $^1S_0$ pp FSI.

The invariant mass distributions of the ϕp system obtained in this experiment and in the previous one at $\varepsilon_\phi = 18.5$ MeV are presented in Fig. 7. For both energies the data differ significantly from uniform phase-space predictions (dashed curve). Calculations that include in addition the pp final state interaction (dotted curve) can describe the data at $\varepsilon_\phi = 18.5$ MeV, but fail at $\varepsilon_\phi = 76$ MeV, where the higher partial waves of Eq. (2) are successful (solid curve).

IV. THE TOTAL CROSS SECTIONS

The peaking at low IM$_{K^+K^-}$ in the raw K^+K^- invariant mass distribution of Fig. 2 is mainly a consequence of the ANKE acceptance and a smoother behavior in this region is seen in the acceptance-corrected data in Fig. 8. The contributions are there shown separately for the ϕ and non-ϕ contributions. Away from the low-mass region the latter resembles quite closely that of a four-body ppK^+K^- phase space, which is also shown.

The fit to the acceptance-corrected invariant mass distribution of Fig. 8 was used to determine separately the total cross sections for ϕ and non-ϕ production measured in the $pp \to ppK^+K^-$ reaction at 2.83 GeV. These results, together with our previous ones at this energy, are summarized in Table III. The two data sets are consistent within statistics, though the precision of the current one is much higher. It should be noted that the total cross section for ϕ production was corrected for the branching ratio $\Gamma_{K^+K^-}/\Gamma_{\text{tot}} = 0.491$ [30].

The total cross section for the $pp \to pp\phi$ reaction is plotted in Fig. 9(a) alongside other existing near-threshold data

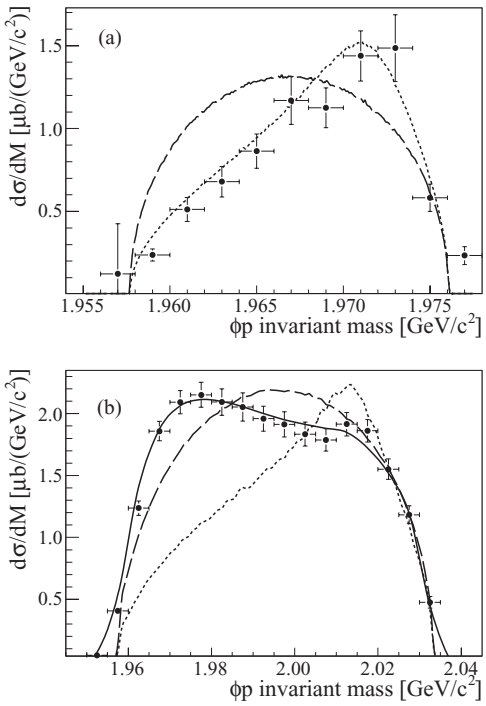

FIG. 7. The acceptance-corrected differential cross section as a function of the ϕp invariant mass at excess energies (a) $\varepsilon_\phi =$ 18.5 MeV and (b) $\varepsilon_\phi = 76$ MeV. The dashed curves show phase-space predictions, while the dotted cures include the pp FSI. The solid curve represents the description of Eq. (2), with parameters being taken from Table. I.

[15,17] as a function of the excess energy ε_ϕ. The error bars shown are quadratic sums of the systematic and statistical uncertainties. If the coefficients $A_{L\ell}$ were constant, apart from the explicit momentum factors in Eq. (2), then these could be used to predict the energy dependence of the total cross section. The resulting black solid curve, which by construction passes through the 76-MeV point, underestimates severely the low energy data. This behavior comes about because at 76 MeV the fit indicates that only a small fraction of the total cross section corresponds to an Ss final state and, as seen in Fig. 9(a), the contributions from the higher partial waves decrease faster as threshold is approached. It therefore seems that there must be a strong energy variation in some of the $A_{L\ell}$, which might be driven by a ϕp near-threshold enhancement.

TABLE III. Total cross section for the $pp \to ppK^+K^-$ reaction at $T_p = 2.83$ GeV separated into ϕ and non-ϕ components. In the ϕ case the data have been corrected for the $\phi \to K^+K^-$ branching ratio. The uncertainties are, respectively, statistical and systematic. The results of previous measurements [15,16] are also given.

Channel	σ[nb]	σ[nb] [15,16]
Non-ϕ production	$91.0 \pm 3.0 \pm 11.4$	$98.0 \pm 8.0 \pm 15.0$
ϕ production	$142.2 \pm 2.1 \pm 17.9$	$133.0 \pm 12.0 \pm 27.0$
Total K^+K^-	$160.8 \pm 3.2 \pm 14.4$	$163.3 \pm 10.0 \pm 20.0$

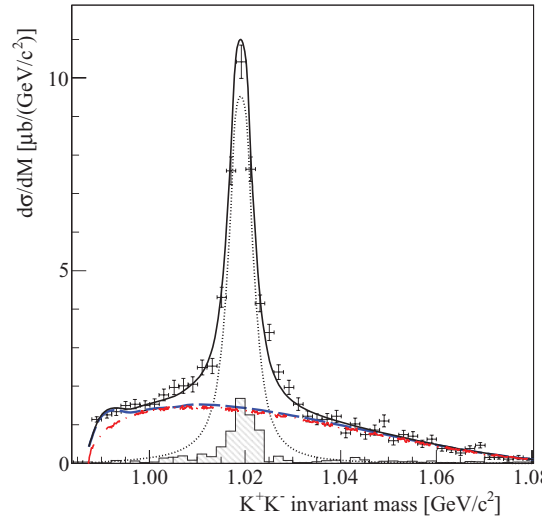

FIG. 8. (Color online) The acceptance-corrected $pp \to ppK^+K^-$ differential cross section as a function of the K^+K^- invariant mass. The error bars correspond only to the statistical uncertainties; systematic uncertainties are shown by the hatched histograms. The dashed blue curve shows the non-ϕ contributions within the fitted parametrization, the dashed-dotted red curve the four-body phase-space simulation of ppK^+K^-, and the dotted curve the ϕ contributions. The solid line is the incoherent sum of the ϕ and non-ϕ contributions.

The energy dependence of the total cross section is close to the predictions from Kaptari and Kämpfer [9], which include mesonic and nucleonic current contributions. The predictions are very similar to those of three-body phase space modified by the effects of the pp FSI. This curve can fit most of the data in Fig. 9(b) because, unlike the Ss curve, it takes the full strength at 76 MeV. The model of Tsushima and Nakayama [11] also includes both nucleonic and mesonic current contributions but gives too steep an energy dependence. In neither model were contributions from nucleon resonances considered which, if they existed, would change the energy dependence of the $A_{L\ell}$. Also shown are the predictions of the resonance model of Xie *et al.* [13]. For ease of comparison, these have all been scaled to pass through the 76-MeV point. On the other hand, the one-pion-exchange calculation [7], which fits the ϕ production results at high energy ($\varepsilon_\phi > 1$ GeV), fails to describe any of the near-threshold data. The model was subsequently extended through the inclusion of baryonic resonances with masses close to the ϕp threshold [14]. This achieves a better description at lower energies, as shown in Fig. 9(b). It is clear from this discussion that the behavior of the total cross sections is insufficient by itself to distinguish between different theoretical models; such calculations must be tested against various differential spectra of the types presented here.

The current value of the $pp \to pp\phi$ total cross section at 76 MeV given in Table III is only a little higher than our previous result [16]. The conclusion drawn there, that the ratio of this to the cross section for ω production is about a factor of six above the OZI limit [2], is therefore still valid.

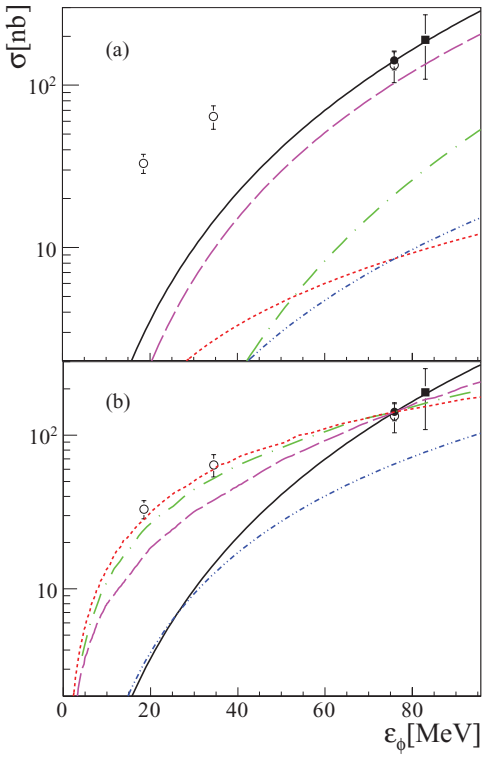

FIG. 9. (Color online) Total cross section for the $pp \to pp\phi$ reaction as a function of excess energy ε_ϕ. The present result (solid circle) is shown together with experimental data taken from DISTO [17] (solid square) and previous ANKE measurements [15] (open circles). (a) The data are compared to the black solid curve derived using Eq. (2) with the parameters taken from Table I. The individual contributions from the Ss (dotted red curve), Sp (double dotted-dashed blue curve), Ps (dashed magenta curve), and Pp (dashed-dotted green curve) are normalized to their predicted values at 76 MeV. (b) The predictions of Tsushima and Nakayama [11] (dashed magenta), scaled to pass through the 76 MeV point, underestimate the low energy data. Also shown are the predictions of Kaptari and Kämpfer [9] (dashed-dotted green), which are very similar to those of three-body phase space with the inclusion of the pp FSI, and a one-pion-exchange model of Sibirtsev [7] (double dotted-dashed blue), and this plus exotic baryons [14] (dotted red), and the results within a resonance model Xie *et al.* [13] are indistinguishable from the calculation with exotic baryons [14].

Values of the non-ϕ contribution to the $pp \to ppK^+K^-$ total cross section were reported in our earlier work [16] and any change in the 76-MeV point is well within the total error bars. It was shown there that the energy dependence of this cross section could only be understood fully if all the final state interactions in the pp, K^-p, and K^+K^- subsystems were included in the estimates.

V. NON-ϕ INVARIANT MASS DISTRIBUTIONS

The strong K^-p interaction can distort hugely both the K^-p and K^-pp invariant mass distributions, and this is taken into account through Eq. (1). The effects are most apparent if one forms the ratios of the differential cross sections in terms

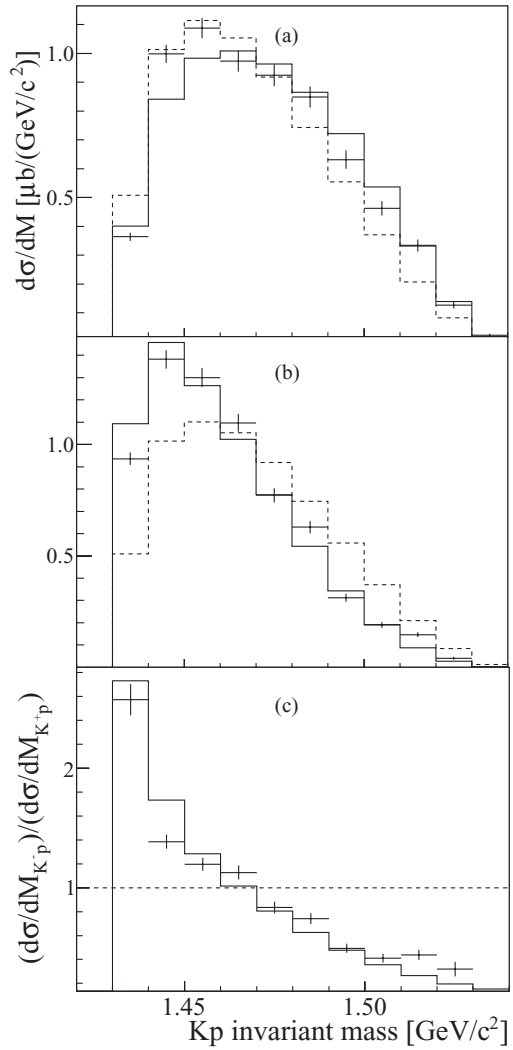

FIG. 10. Differential cross sections for the $pp \to ppK^+K^-$ reaction in the non-ϕ region with respect to the invariant masses of K^+p (a) and K^-p (b), and their ratio R_{Kp} (c). The dashed histograms represent the four-body phase-space simulations, whereas the solid ones represent the theoretical calculations taking into account pp and K^-p final state interactions through Eq. (1).

of the invariant masses:

$$R_{Kp} = \frac{d\sigma/dM_{K^-p}}{d\sigma/dM_{K^+p}}, \quad R_{Kpp} = \frac{d\sigma/dM_{K^-pp}}{d\sigma/dM_{K^+pp}}. \tag{6}$$

The corresponding experimental data and simulations are to be found in Figs. 10 and 11. If the K^+p and K^-p final state interactions were identical, then the ratios R_{Kp} and R_{Kpp} would be constant and equal to unity. However, both R_{Kp} and R_{Kpp} display very large preferences for lower invariant masses, which probably reflect an attraction between the K^- and one or both of the protons. Similar effects have been observed at lower excess energies [16,20,21].

The general features of these results are well reproduced by the simple factorized ansatz of Eq. (1). It is nevertheless surprising that the distortions produced by the constant effective scattering length, $a = (0 + 1.5i)$ fm, used at $\varepsilon_{KK} = 51$ MeV [16] still describe the data so well at an excess energy

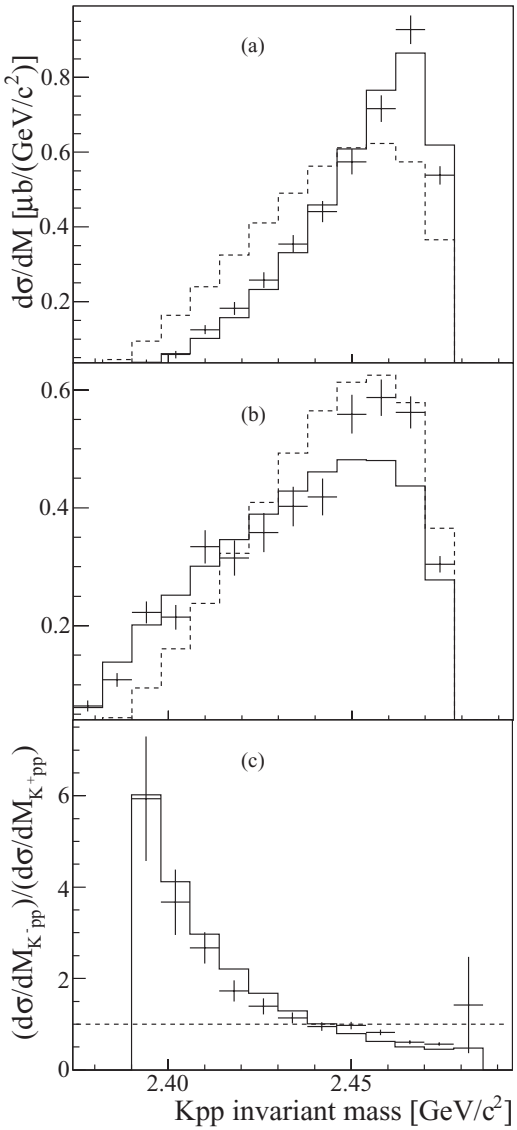

FIG. 11. Differential cross sections for the $pp \to ppK^+K^-$ reaction in the non-ϕ region with respect to the invariant masses of K^+pp (a) and K^-pp (b), and their ratio R_{Kpp} (c). The dashed histograms represent the four-body phase-space simulations, whereas the solid ones represent the theoretical calculations taking into account pp and K^-p final state interactions through Eq. (1).

with respect to the K^+K^- threshold as high as 108 MeV, though some deviations are apparent for Kp invariant masses above about 1.5 GeV/c^2.

The distortions of Figs. 10 and 11 clearly indicate that the direct production of the scalar resonance a_0 or f_0 cannot be the dominant driving mechanism in the $pp \to ppK^+K^-$ reaction. On the other hand, the strength of the K^-p interaction suggests that kaon pair production might be related to that of the $\Lambda(1405)$ through $pp \to pK^+(\Lambda(1405) \to K^-p)$ [1]. This idea was put on a quantitative footing by assuming that the $\Lambda(1405)$ was formed through the decay $N^\star \to K^+\Lambda(1405)$ [33].

The simple ansatz of Eq. (1) underestimates the cross section for low K^+K^- masses (i.e., in the interval between the

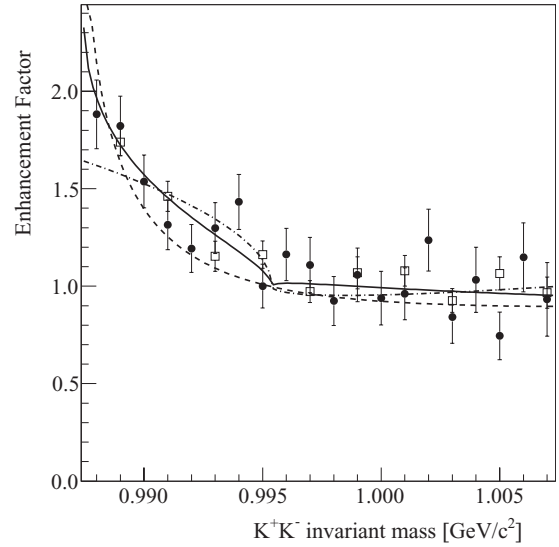

FIG. 12. Ratio of the measured K^+K^- invariant mass in the $pp \to ppK^+K^-$ reaction to estimates based on Eq. (1). In addition to the current data (solid circles), the weighted averages of previous measurements (open squares) [16] are also presented. The solid curve represents the best fit in the model of Ref. [28], which includes charge-exchange and elastic K^+K^- FSI. The best fits neglecting charge exchange and including only this effect are shown by the dashed and the dot-dashed curve, respectively.

K^+K^- and $K^\circ\bar{K}^\circ$ thresholds at 987.4 and 995.3 MeV/c^2, respectively). Similar effects were observed in $pp \to ppK^+K^-$ by DISTO [17] and by ANKE in $pn \to dK^+K^-$ [34]. Although these enhancements must be from $K\bar{K}$ final state interactions, including $K^+K^- \rightleftharpoons K^0\bar{K}^0$ charge exchange scattering, they could be connected with some small production of the a_0/f_0 scalar resonances. However, in reality, the data are only sensitive to the $K\bar{K}$ scattering lengths.

A combined analysis of ANKE data at three energies [28] suggests that, independent of the exact values of the scattering lengths, the $K\bar{K}$ enhancement is mainly in the isospin-zero channel. The model for the enhancement factor fitted there was introduced into the simulation to describe better the data shown in Fig. 8 for invariant masses $\mathrm{IM}_{KK} < 995$ MeV/c^2. Its effects can be seen more clearly in the plot of the ratio of the K^+K^- invariant-mass data to the simulation based on Eq. (1), where no $K\bar{K}$ FSI was included. This, together with the results of previous measurements [16], are shown in Fig. 12. The two data sets are in agreement and are consistent with the existence of some coupled-channel effect at the $K^0\bar{K}^0$ threshold but much better data would be required to prove this unambiguously.

VI. DISCUSSION AND CONCLUSIONS

New measurements of the differential and total cross sections for the production of kaon pairs in proton-proton collisions have been presented at a beam energy of 2.83 GeV. The reaction was identified through a triple coincidence of a K^+K^- pair and a forward-going proton detected in the

COSY-ANKE magnetic spectrometer, with an additional cut being placed on the missing-mass spectrum.

By careful modeling, it was possible to describe all the experimental spectra in regions of the K^+K^- invariant mass where the ϕ meson sits, as well as at smaller and larger masses. This allowed acceptance corrections to be made to extract cross sections where the ϕ and non-ϕ contributions were reliably separated.

The main feature of the non-ϕ data is the very strong distortion of both the K^-p and K^-pp spectra by the K^-p final state interaction. This may be a reflection of the excitation of the $\Lambda(1405)$ in the production process and, in the Xie and Wilkin approach [33], the production of non-ϕ kaon pairs proceeds mainly through the excitation of K^+-hyperon pairs. It is remarkable to note that these distortions are described quantitatively by the factorized approximation of Eq. (1) with the same constant scattering length that was used for the lower energy data [16]. On the other hand, because these data correspond to events where the K^+K^- emerge in the final state, they cannot contribute directly to the ongoing debate regarding the possibility of deeply bound K^-pp states [35], except to emphasize that the K^-pp interaction is still strong even above threshold.

There is evidence for some K^+K^- final state interaction that changes in nature at the $K^0\bar{K}^0$ threshold but the contribution of this region to the integrated $pp \to ppK^+K^-$ cross section is very small and it is hard to find any indication of the excitation of the a_0/f_0 scalar resonances in the reaction. As already pointed out in our earlier work [16], the energy dependence of the total cross section near threshold can be understood simply in terms of the effects of the pp, K^-p, and K^+K^- FSI. To establish a better understanding of possible structure at the $K^0\bar{K}^0$ threshold, high statistics are required in this region and this might be achieved in the data collected below ϕ production threshold [36].

Having a good description of the background, it was possible to derive detailed invariant mass and angular distributions for the $pp \to pp\phi$ reaction. Although the DISTO collaboration [17] showed the significance of higher partial waves at the marginally higher excitation energy of $\varepsilon_\phi = 83$ MeV, they did this mainly on the basis of relative momentum spectra. Their conclusion is confirmed unambiguously by the angular distributions presented here. For example, at $\varepsilon_\phi = 18.5$ MeV the ϕ meson is completely aligned, as it has to be for a Ss final state [15]. In contrast, in the present data the emerging ϕ is almost unpolarized and this clearly signals the presence of higher partial waves. This is consistent with the evidence from the momentum distributions, which also show the dominance of P waves in the final pp system. This explains why the $^1S_0$ pp FSI, which is so important at $\varepsilon_\phi = 18.5$ MeV [15], is not observed at 76 MeV. Furthermore, in contrast to the DISTO result [17], clear anisotropy was observed in the ϕ c.m. angular distribution and this can be ascribed to the contribution from the p wave. This angular distribution might provide information on nucleonic current contributions and the $NN\phi$ coupling constant [10,11].

Even if one considers only a few partial waves, there are simply too many parameters to perform useful fits and only typical Ss, Sp, Ps, and Pp contributions were considered in Eq. (2). The fitted data show that the contribution of the final Ss wave to the cross section represents only a small amount of the total at $\varepsilon_\phi = 76$ MeV. As a consequence, the extracted parameters predict a total cross section that grossly underestimates the measurements at lower energies.

The simplest way out of the total cross-section dilemma would be to assume that a ϕp threshold enhancement leads to a significant energy dependence of some of the $A_{L\ell}$ coefficients. In this context it is interesting to note that the large contribution of the Pp wave to the $pp \to pp\eta$ cross section at an excess energy of 72 MeV was ascribed to a strong ηp FSI driven by the $N^*(1535)$ isobar [37]. Against the ϕp enhancement hypothesis is the fact that the large excess of events in the ϕp invariant mass distribution shown in Fig. 7(b) at low masses can be explained in the partial wave fitting of Eq. (2), without including any ϕp enhancement. We have not, however, shown that the fitting of the data is unambiguous and there could be other truncated partial wave forms that might be equally successful. Furthermore, from the start we have not included any final state interaction between the ϕ and the protons in the parametrization. There could therefore be a possible trade-off between some of the partial wave parameters and an FSI in the ϕp system. Nevertheless, the phenomenological parametrization is sufficient for acceptance correction and it describes most of the differential distributions quite well.

In the parametrization of Eq. (2), the coefficients $A_{L\ell}$ were taken to be constant and no resonance effects were included. Recent theoretical studies have suggested that bound states or resonances might be formed in the near-threshold ϕp system [38,39] and, if so, they would certainly influence the behavior of some of the $A_{L\ell}$. In this context, it is interesting to note that a bump was observed in the near-threshold ϕ meson photoproduction from hydrogen by LEPS [40] and in the preliminary results of CLAS [41]. Furthermore, it seems that s-wave production of the ϕ in the $pd \to {}^3\mathrm{He}\,X$ reaction is anomalously large compared to the ω and η' mesons [42]. Such effects might even be part of the explanation for the violation of the OZI rule [2] in the ratio of ϕ to ω production. Alternatively, it is possible that other strangeness production channels could influence the energy dependence of the $pp \to ppK^+K^-$ reaction [43–45].

Although some theoretical models have been able to describe *a posteriori* the published total cross sections for ϕ production, calculations of differential distributions with which to compare our experimental data are somewhat limited. It is only when a model is tested against a range of differential distributions, as presented here, that some credence can be given to the model. Total cross sections are insufficient and more theoretical work is therefore required.

ACKNOWLEDGMENTS

We thank the COSY machine crew for their continued assistance as well as that of other members of the ANKE Collaboration. Discussions with J. Haidenbauer, C. Hanhart, K. Nakayama, and A. Sibirtsev were very helpful. This work was supported in part by the US Department of Energy under Contract No. DE-FG02-03ER41231, and the BMBF, DFG, Russian Academy of Sciences, and COSY FFE.

[1] C. Wilkin, Acta Phys. Polon. Suppl. **2**, 89 (2009).
[2] S. Okubo, Phys. Lett. **5**, 165 (1963); G. Zweig, CERN Report No. TH-401, 1964; J. Iizuka, Prog. Theor. Phys. Suppl. **37-38**, 21 (1966).
[3] C. Amsler *et al*., Rev. Mod. Phys. **70**, 1293 (1998).
[4] M. P. Locher and Y. Lu, Z. Phys. A **351**, 83 (1995).
[5] U.-G. Meißner *et al*., Phys. Lett. B **408**, 381 (1997).
[6] A. Polyanskiy *et al*., Phys. Lett. B **695**, 74 (2011); M. Hartmann *et al*., Phys. Rev. C **85**, 035206 (2012).
[7] A. Sibirtsev, Nucl. Phys. A **604**, 455 (1996).
[8] A. I. Titov, B. Kämpfer, and V. V. Shklyar, Phys. Rev. C **59**, 999 (1999); A. I. Titov, B. Kämpfer, and B. L. Reznik, Eur. Phys. J. A **7**, 543 (2000).
[9] L. P. Kaptari and B. Kämpfer, Eur. Phys. J. A **23**, 291 (2005).
[10] K. Nakayama, J. W. Durso, J. Haidenbauer, C. Hanhart, and J. Speth, Phys. Rev. C **60**, 055209 (1999).
[11] K. Tsushima and K. Nakayama, Phys. Rev. C **68**, 034612 (2003).
[12] A. Faessler, C. Fuchs, M. I. Krivoruchenko, and B. V. Martemyanov, Phys. Rev. C **68**, 068201 (2003); **70**, 035211 (2004).
[13] J. J. Xie, B. S. Zou, and H. C. Chiang, Phys. Rev. C **77**, 015206 (2008).
[14] A. Sibirtsev, J. Haidenbauer, and U.-G. Meißner, Eur. Phys. J. A **27**, 263 (2006).
[15] M. Hartmann *et al*., Phys. Rev. Lett. **96**, 242301 (2006).
[16] Y. Maeda *et al*., Phys. Rev. C **77**, 015204 (2008).
[17] F. Balestra *et al*., Phys. Rev. C **63**, 024004 (2001).
[18] M. Wolke, Dissertation, Westfälische Wilhelms-Universität Münster, 1998.
[19] C. Quentmeier *et al*., Phys. Lett. B **515**, 276 (2001).
[20] P. Winter *et al*., Phys. Lett. B **635**, 23 (2006).
[21] M. Silarski *et al*., Phys. Rev. C **80**, 045202 (2009).
[22] R. Maier *et al*., Nucl. Instrum. Meth. Phys. Res. A **390**, 1 (1997).
[23] S. Barsov *et al*., Nucl. Instrum. Meth. Phys. Res. A **462**, 364 (2001).
[24] M. Hartmann *et al*., Int. J. Mod. Phys. A **22**, 317 (2007).
[25] S. Dymov *et al*., Part. Nucl. Lett. **2**, 40 (2004) [http://www1.jinr.ru/Pepan_letters/panl_2_2004/2_2004_05_dym.pdf].
[26] A. Khoukaz *et al*., Eur. Phys. J. D **5**, 275 (1999).
[27] M. Büscher *et al*., Nucl. Instrum. Meth. Phys. Res. A **481**, 378 (2002).
[28] A. Dzyuba *et al*., Phys. Lett. B **668**, 315 (2008).
[29] S. Agostinelli *et al*., Nucl. Instrum. Meth. Phys. Res. A **506**, 250 (2003); [http://geant4.web.cern.ch/geant4].
[30] K. Nakamura *et al*., J. Phys. G **37**, 075021 (2010).
[31] Y. Maeda *et al*., Phys. Rev. Lett. **97**, 142301 (2006).
[32] M. Abdel-Bary *et al*., Eur. Phys. J. A **44**, 7 (2010).
[33] J. J. Xie and C. Wilkin, Phys. Rev. C **82**, 025210 (2010).
[34] Y. Maeda *et al*., Phys. Rev. C **79**, 018201 (2009).
[35] T. Yamazaki *et al*., Phys. Rev. Lett. **104**, 132502 (2010).
[36] M. Hartmann *et al*., COSY Proposal **191** (2008), [www2.fz-juelich.de/ikp/anke/en/proposals.shtml].
[37] H. Petrén *et al*., Phys. Rev. C **82**, 055206 (2010).
[38] H. Gao, T.-S. H. Lee, and V. Marinov, Phys. Rev. C **63**, 022201 (2001).
[39] J. Yamagata-Sekihara, D. Cabrera, M. J. Vicente Vacas, and S. Hirenzaki, Prog. Theor. Phys. **124**, 147 (2010).
[40] T. Mibe *et al*., Phys. Rev. Lett. **95**, 182001 (2005).
[41] B. Dey *et al*., AIP Conf. Proc. **1388**, 242 (2011).
[42] G. Fäldt and C. Wilkin, Phys. Lett. B **354**, 20 (1995).
[43] B. Dey *et al*., Phys. Rev. C **82**, 025202 (2010).
[44] S. A. Pereira *et al*., Phys. Lett. B **688**, 289 (2010).
[45] H. Kohri *et al*., Phys. Rev. Lett. **104**, 172001 (2010).